land

MDPI

Article

Remotely-Sensed Surface Temperature and Vegetation Status for the Assessment of Decadal Change in the Irrigated Land Cover of North-Central Victoria, Australia

Mohammad Abuzar [1,*], Andy McAllister [2], Des Whitfield [2] and Kathryn Sheffield [1]

1 Agriculture Victoria Research, Department of Jobs, Precincts and Regions (DJPR), AgriBio, 5 Ring Road, Bundoora 3083, Australia; kathryn.sheffield@agriculture.vic.gov.au
2 Agriculture Victoria Research, Department of Jobs, Precincts and Regions (DJPR), 255 Ferguson Road, Tatura 3016, Australia; andy.mcallister@agriculture.vic.gov.au (A.M.); des.whitfield@agriculture.vic.gov.au (D.W.)
* Correspondence: mohammad.abuzar@agriculture.vic.gov.au

Received: 2 August 2020; Accepted: 29 August 2020; Published: 2 September 2020

check for updates

Abstract: Monitoring of irrigated land cover is important for both resource managers and farmers. An operational approach is presented to use the satellite-derived surface temperature and vegetation cover in order to distinguish between irrigated and non-irrigated land. Using an iterative thresholding procedure to minimize within-class variance, the bilevel segmentation of surface temperature and vegetation cover was achieved for each irrigation period (Spring, Summer and Autumn). The three periodic profiles were used to define irrigation land covers from 2008–2009 to 2018–2019 in a key agricultural region of Australia. The overall accuracy of identifying farms with irrigated land cover amounted to 95.7%. Total irrigated land cover was the lowest (approximately 200,000 ha) in the 2008–2009 crop year which increased more than three-fold in 2012–2013, followed by a gradual decline in the following years. Satellite images from Landsat series (L-5, L-7 and L-8), Sentinel-2 and ASTER were found suitable for land cover classification, which is scalable from farm to regional levels. For this reason, the results are desirable for a range of stakeholders.

Keywords: land cover; irrigation; satellite images; agriculture; remote sensing

1. Introduction

Irrigated agriculture is a vital source of food and fiber [1–3]. Recently there has been an increasing reliance on irrigated agriculture worldwide as the dryland agriculture has been adversely impacted by climatic changes [4]. Irrigated agriculture uses a large proportion of available freshwater globally, amounting for about 70% [2,5]. In the face of competing demands for limited water resources, there is a sharp focus on the management of irrigated agriculture [6]. The mapping and monitoring of accurate irrigated land cover is vitally important for effective irrigation management and judicious decision making.

The past few decades have witnessed a wide application of Remote Sensing for mapping cropland [3,7,8]. Several studies have adopted standard procedures of different classification techniques for mapping at various spatial scales, including regional [9–12] and continental [9,11,13,14] levels. There is an increasing interest in cropland mapping at global scale utilizing high frequency coarse resolution data sets from various sensors/satellites including MODIS, AVHRR, MERIS and SPOT VGT [15,16]. Mapping irrigated agriculture and assessing irrigation activities is not common at a global or regional level [17]. There are very few studies on operational approaches to map and monitor irrigated agriculture on a routine basis [18,19]. Some recent reviews have adequately summarized the current status of Remote Sensing applications to agricultural mapping [3,7,18]. Studies on irrigated agriculture are notably far more scarce as compared to agriculture in general. What most studies on irrigated cropland have done so far is to delineate the usual 'irrigation' areas, which is not the same as the actually 'irrigated' land within an irrigation period. In order to investigate periodic or in-season variation in irrigation, it is important to identify the land cover which is actually 'irrigated' with sufficient spatial detail, which has been attempted in this study.

Since the earliest attempts to develop vegetation indices in 1960s–1970s [20,21], many new and modified indices have been researched that relate to plant parameters [8]. Most of these vegetation indices use the combination of spectral responses between visible and the near- or mid-infrared range. However, the most widely used measure is the normalized difference vegetation index (NDVI), which is based on two spectral bands (near infrared and red). Vegetation indices including NDVI have been used in mapping agricultural land cover. However, for irrigated land cover, surface wetness is required as additional information. Surface temperature has been recognized as an indicator of surface moisture and crop water [22]. The differences in surface temperature are potential indicators of irrigation variations [7,13,19]. However, there is a lack of detailed studies using temperature information for irrigation mapping [7]. The objective of this study was: (a) to map irrigated areas for each season by using satellite-based surface temperature and NDVI; (b) to identify land cover classes by using the seasonal profile of irrigated areas; and (c) to evaluate the changes in irrigated land cover over ten years (2008–2009 to 2018–2019) in a key irrigation region located in the northern part of Victoria, Australia. For the accuracy assessment of our mapped irrigated areas, we used information on irrigation water deliveries of a recent season to determine whether the farms were actually irrigated or not within that season.

2. Study Area

The study area is located approximately between 35.14° S and 36.71° S latitudes, and between 143.31° E and 146.03° E longitudes in the north-central part of Victoria, Australia (Figure 1). With the Murray River in the north, it is spread over the river catchments of Goulburn-Broken, Campaspe and Loddon. It covers an area of about 9950 sq km. About 75% of the land is irrigated. Of the total irrigated land, 87% is used for pastures, 4% for treed horticulture crops and the remaining 9% is used for other purposes including vegetables and grain crops. The climate is temperate, and the region is relatively dry with average annual rainfall of between 300 mm and 500 mm. Generally, winters (June to August) are wet, receiving most of the annual rainfall. Summers (December to February) are usually dry and are when the demand for supplemental water for crops is the highest. Irrigation demand during Spring (September to November) and Autumn (March to May) is variable. The major agricultural industries are dairy, and stone and pome fruit production. The flat terrain and shallow natural drainage of the region are overlaid by a network of irrigation channels. Multiple irrigation system configurations are used in the region including micro-irrigation, conventional sprinkler, flood and furrow.

For management purposes, the irrigation region is divided into six sub-regions or 'irrigation areas' [23] as shown in Figure 1B: Central Goulburn, Shepparton, Murray Valley, Campaspe, Pyramid–Boort and Torrumbarry.

3. Materials and Methods

In this study, we present an operational approach to use satellite-based surface temperature and vegetation status to map irrigated areas with enough spatial detail and to monitor land cover changes. We introduce an approach to incorporate the relative differences of surface temperature with NDVI to map the areas of irrigated agriculture [24]. The operational approach adopted in this study was firstly to process the satellite images and generate surface temperature (Ts) and NDVI. Secondly, to identify relative differences of Ts and NDVI, appropriate thresholds were determined. At this stage, seasonal matrices of individual pixel profiles based on Ts and NDVI were compiled.

As a third step, irrigated land cover classes were generated using seasonal profiles of pixels, and maps were created for each crop year (September–May). Finally, temporal changes in the irrigated land covers were evaluated.

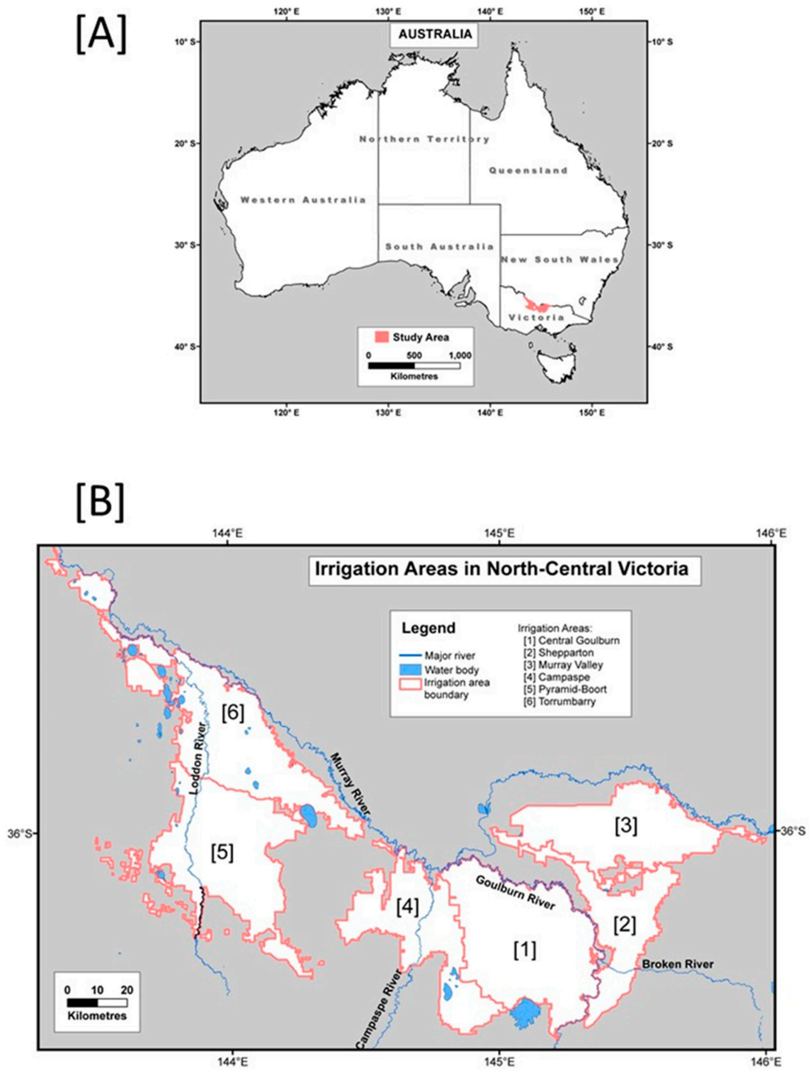

Figure 1. Map of the study area. (**A**) Location of the study area in Australia; (**B**) Map showing irrigation areas (sub-regions) in North-Central Victoria.

3.1. Step 1: Data Preparation

Satellite images were collected to represent the three irrigation periods (Spring, Summer and Autumn) of every crop year during 2008–2009 to 2018–2019 seasons, except the three crop years (2010–2011, 2011–2012 and 2016–2017) when there was no suitable imagery available over the study area, which have been excluded from the study (Table 1). Most of the data sets were acquired from three Landsat satellites (L5, L7 and L8) sourced from USGS (https://earthexplorer.usgs.gov/). Data gaps were filled using ASTER (https://search.earthdata.nasa.gov/) and, to a lesser extent, Sentinel-2 (https://scihub.copernicus.eu/) imagery. To have a complete coverage over the study area, multiple adjacent images were acquired for each season (Figure 2).

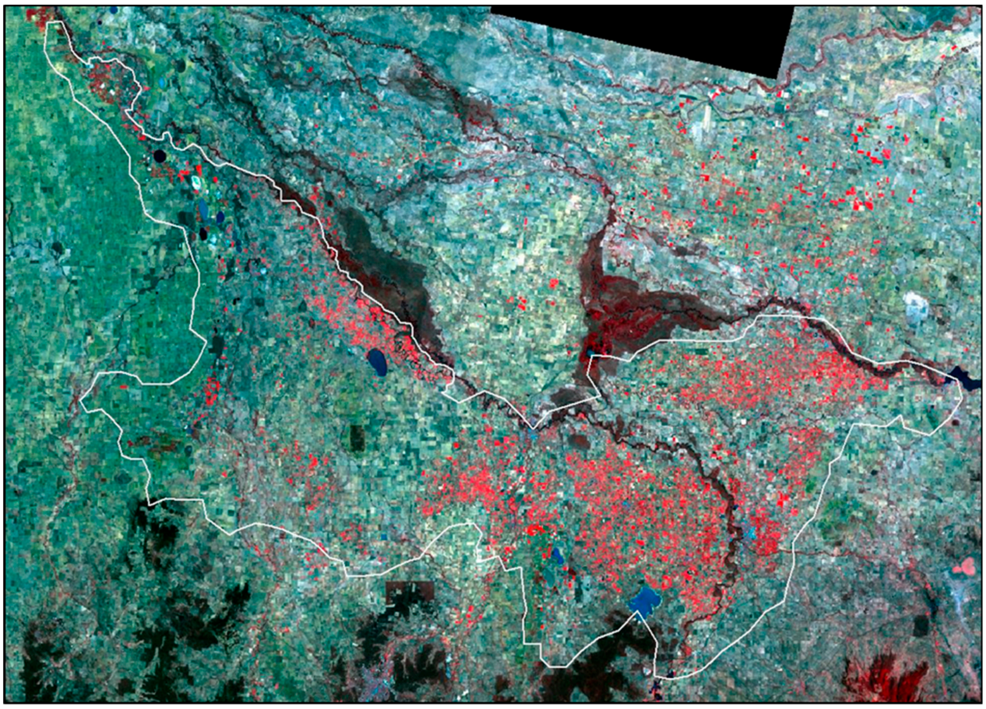

Figure 2. Landsat-8 satellite of summer 2018–2019 is a mosaic of four scenes acquired during January–February 2019 with the band combination of 543 (Red, Green, Blue). White boundary indicates the extent of the study area.

For vegetation status, NDVI was calculated using reflectance of near infrared (NIR) and red spectral bands [25]:

$$\mathrm{NDVI} = \frac{\mathrm{NIR} - \mathrm{RED}}{\mathrm{NIR} + \mathrm{RED}}. \tag{1}$$

Standard procedures were used to calculate reflectance from Landsat series [26,27] and ASTER images [28]. The following formula was used to calculate at-sensor top of the atmosphere (TOA) reflectance:

$$\rho\lambda = \frac{\pi \cdot L_\lambda \cdot d^2}{\mathrm{ESUN}_\lambda \cdot \cos\theta_s} \tag{2}$$

$\rho\lambda$ = Planetary TOA reflectance [-]
π = Mathematical constant equal to ~3.14159 [-]
L_λ = Spectral radiance [W/ (m^2 sr µm)]
d = Earth-Sun distance [Astronomical units]
ESUN_λ= Mean exoatmospheric solar irradiance [W/(m^2 µm)]
θ_s = Solar zenith angle [Degrees].

The downloaded Sentinel-2 images were already converted to reflectance [29]. *Ts* from the Landsat series was calculated using the standard procedures [26,27]. *Ts* as at-sensor brightness temperature was calculated using the following formula:

$$Ts = \frac{K2}{ln\left(\frac{K1}{L_\lambda} + 1\right)} \tag{3}$$

Ts = Effective at-sensor brightness temperature [K]
$K2$ = Calibration constant 2 [K]
$K1$ = Calibration constant 1 [W/ (m^2 sr µm)]

L_λ = Spectral radiance at the sensor's aperture [W/ (m^2 sr µm)]
ln = Natural logarithm.

Surface temperature from ASTER was calculated using band TIR4 (10.25–10.95 µm) [28]. NDVI from ASTER and Sentinel-2 as well as Ts from ASTER were re-sampled to a 30 m resolution using bilinear interpolation method and were adjusted to be comparable to Landsat equivalents. The adjustment factors used in this study were taken from our previous investigations [24,30].

Table 1. List of satellite images used.

Season/Year	Western Part (WRS-2: 94/84-85)	Central Part (WRS-2: 93/85)	Eastern Part (WRS-2: 92/85)
Spring 2008	L5: 10 October 2008	L5: 4 November 2008	L5: 28 October 2008
Summer 2008–2009	L5: 14 January 2009	L5: 23 January 2009	L5: 16 January and 1 February 2009
Autumn 2009	L5: 20 April 2009	L5: 13 April 2009	L5: 8 May 2009
Spring 2009	L5: 11 September 2009	L5: 22 October 2009	L5: 31 October 2009
Summer 2009–2010	L5: 16 December 2009	L5: 9 December 2009 and 11 February 2010	L5: 18 December 2009
Autumn 2010	L5: 22 March 2010	L5: 2 May 2010	L5: 25 April 2010
Spring 2012	L7: 11 September and 14 November 2012	L7: 4 September and 22 October 2012	ASTER: 15 October 2012
Summer 2012–2013	L7: 17 January, 2 February and 18 February 2013	L7: 10 and 26 January, and 11 February 2013 ASTER: 9 and 18 December 2012; 1, 3 and 10 January 2013	L7:2 January and 3 February 2013
Autumn 2013	L8: 15 April 2013	L7:16 April and 2 May 2013	L7: 11 May 13 L8: 19 May 2013
Spring 2013	L8: 22 September 2013	L8: 18 November 2013	L8: 27 November 2013
Summer 2013–2014	L8: 28 January 2014	L8: 21 January 2014	L8: 30 January 2014
Autumn 2014	L8: 18 April and 4 May 2014	L8: 27 April and 13 May 2014	L8: 6 May 2014
Spring 2014	L8: 11 October 2014	L8: 5 November 2014	L8: 29 October 2014
Summer 2014–2015	L8: 16 February 2015	L8: 9 February 2015	L8: 2 February 2015
Autumn 2015	L8: 21 April 2015	L8: 16 May 2015	L8: 10 June 2015 L7: 1 and 17 May 2015
Spring 2015	L8: 14 October 2015	L8: 23 October 2015	L7:24 October and 9 November 2015
Summer 2015–2016	L8: 18 January 2016	L8: 12 February 2016	L8: 5 February 2016
Autumn 2016	L8: 23 April 2016	S2: 6 May 2016	25 April 2016
Spring 2017	L8: 4 November 2017	L8: 13 November 2017	S2: 4 November 2017
Summer 2017–2018	L8: 23 January 2018	L8: 17 February 2018	L8: 26 February 2018
Autumn 2018	L8: 29 April 2018	L8: 8 May 2018	L8: 1 May 2018
Spring 2018	L8: 22 October 2018	L8: 31 October and 16 November 2018	L8: 8 and 24 October 2018
Summer 2018–2019	L8: 11 and 27 February 2019	L8: 19 January 2019	L8: 12 January 2019
Autumn 2019	L8: 16 April 2019	L8: 25 April 2019	L8: 4 May 2019

Notes: L5 = Landsat-5; L7 = Lansat-7; L8 = Landsat-8; S2 = Sentinel-2.

Ts provides information on vegetation water status [31]. In well-watered irrigation situations, the Ts is often lower than the surrounding air temperature (Ta). In other situations, when vegetation is water-stressed, there is less transpiration and often vegetation surface temperature rises above the surrounding Ta [32]. Therefore, it is considered useful to use the difference between surface and air temperatures (Ts - Ta) to assess vegetation water status in this study. Half-hourly Ta data, close to the time of satellite overpass, was sourced from the Bureau of Meteorology (www.bom.gov.au) for 13 weather stations across and close to the study area. Ta point data sets were rasterized, using the inverse distance weighted (IDW) method to match the Ts extent and spatial resolution. Then surface-air temperature difference (Ts - Ta) at a pixel level was calculated.

3.2. Step 2: Thresholding Process

It is well known that an 'irrigated' crop has high vegetation and low temperature as compared to other land covers within a region. To take this concept further, temperature (Ts - Ta) and vegetation (NDVI) were segmented into two classes each. Temperature classes were referred to as 'irrigated' (low Ts - Ta) and 'non-irrigated' (high Ts - Ta) and vegetation classes were 'crop' (high NDVI) and 'non-crop' (low NDVI). An iterative thresholding method was used to achieve the binary classification by minimizing within-class variance ($\sigma^2{}_{Within}$) [33]:

$$\sigma^2_{Within}(T_i) = \omega_0 \sigma^2_0(T_i) + \omega_1 \sigma^2_1(T_i). \quad (4)$$

Ti is the threshold which varies by iteration i, ω_0 and ω_1 are the weights (proportion of pixels) of the two classes, and $\sigma^2{}_0$ and $\sigma^2{}_1$ are the variance of the two classes of NDVI and Ts - Ta each.

For operational purposes, the thresholding procedure utilized the relationship of $\sigma^2{}_{Within}$ with between-class variance ($\sigma^2{}_{Between}$) and total variance ($\sigma^2{}_{Total}$) [33]:

$$\sigma^2_{Within}(T_i) = \sigma^2_{Total} - \sigma^2_{Between}(T_i) \quad (5)$$

The initial NDVI threshold (α) was taken as 0.4. All pixels >α were considered as 'crop'. Initial temperature threshold (β) was the median value of Ts - Ta. All pixels <β were taken as 'irrigated'. The iteration interval was set at 0.005 within the limit of ±0.025 of the initial NDVI threshold. For temperature, the iteration interval was set 0.1 within the limit of ±0.5 °C of the initial Ts - Ta threshold (i.e., the median). Altogether, 11 iterations each for NDVI and Ts - Ta were performed for each image. Thresholds with minimum $\sigma^2{}_{\text{Within}}$ were used for binary classification.

Figure 3 presents an example of thresholding process for the Landsat-8 image (Scene 93/85) captured on 19 January 2019 at 00:09 UTC (11:09 AM local time).

Binary classes were assigned to each pixel with four combinations, which we termed as pixel identification (PID) as shown in Figure 4. S1 denotes dry conditions with no or low vegetation; S2 denotes wet conditions with low or no vegetation; S3 indicates some vegetation, possibly crops, without irrigation; and S4 denotes vegetation with wet conditions indicating 'irrigated crop/pasture'. All pixels in an image of a season were assigned a PID. Thus, each pixel profile had three PID assignments representing three irrigation periods (Spring, Summer, Autumn) in each crop year.

For accuracy assessment, we used the water supply data of a recent season (2018–2019 summer) as a 'reference'. The mapped 'irrigated crop/pasture' PID (S4) of the same season was taken as an 'estimate'. Information on irrigation water supplies was sourced from the Victorian Water Register (VWR), a state-wide irrigation water database (https://waterregister.vic.gov.au/).

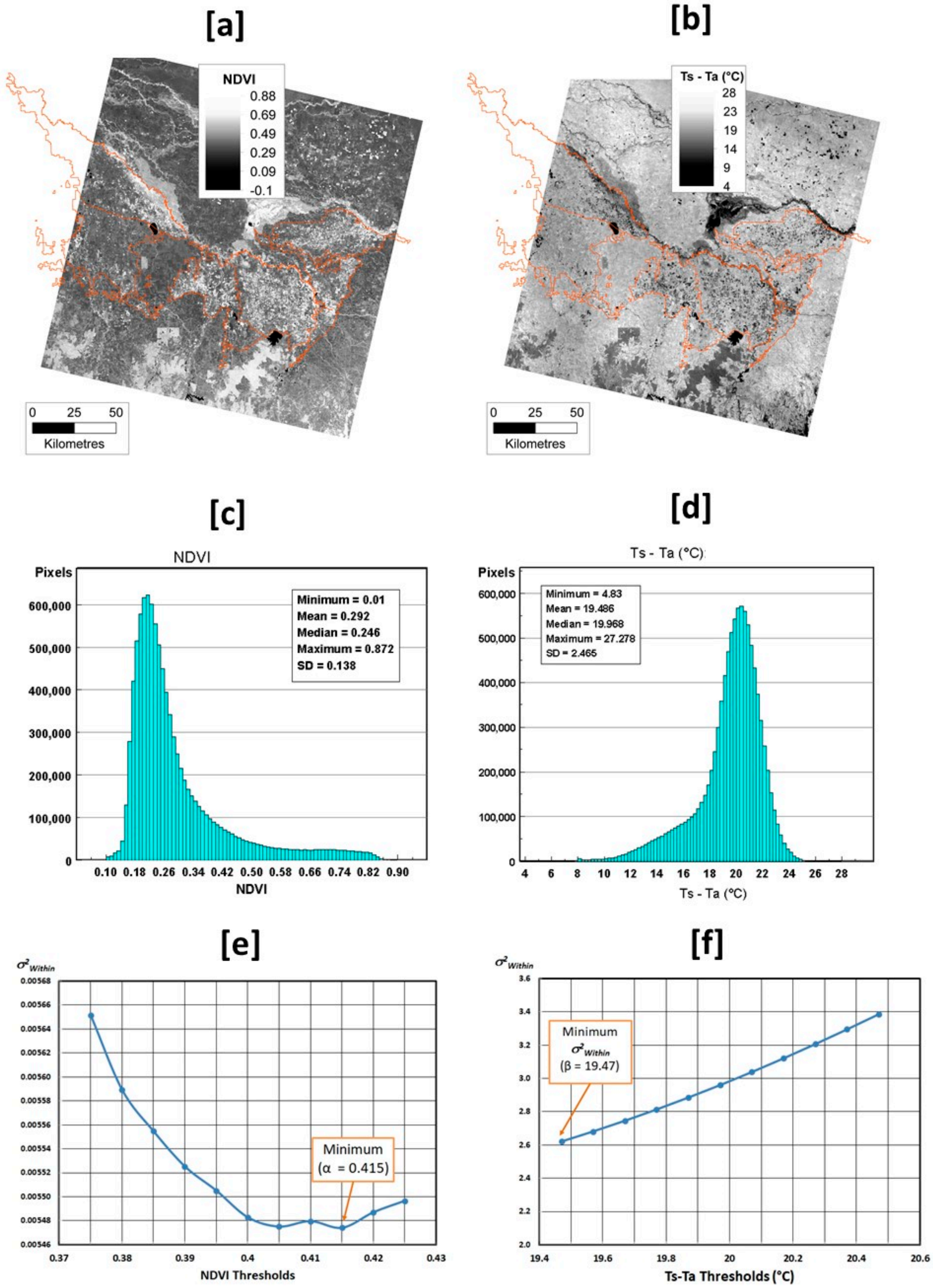

Figure 3. An example of thresholding process based on the Landsat-8 image acquired on 19 January 2019 around 11:09 a.m. (local time), which covers a major central part of the study area. (**a**) normalized difference vegetation index (NDVI) map; (**b**) Map showing Ts - Ta at pixel level; (**c**) Histogram of NDVI; (**d**) Histogram of Ts - Ta; (**e**) Iteration of within-class variance for the NDVI threshold; and (**f**) Iteration of within-class variance for Ts - Ta threshold.

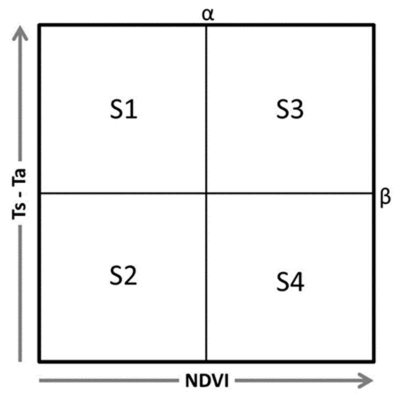

Figure 4. Characterisation of pixels based on NDVI threshold (α) and Ts - Ta threshold (β). S4 denotes irrigated crop/pasture; S3 denotes possible crop or pasture which is not currently irrigated; S2 denotes wet conditions with no or negligible vegetation; and S1 denotes dry conditions with no or negligible vegetation.

3.3. Step 3: Identifying Irrigated Land Cover Classes

Seasonal profiles of pixels were based on NDVI and Ts - Ta binary classes. These pixel profiles provided an indication for each season as to whether or not irrigation was actually applied, and the crop was actively growing. A set of rules were developed to identify irrigated land cover classes (Table 2). Pixels with 'S4' PID were classed as irrigated. However, when some isolated pixels with 'S3' PID were located within or on the border of S4 cluster, those were also recognized as irrigated. Otherwise all pixels with S1, S2 and S3 were recognized as non-irrigated. A contiguity analysis was carried out on the land cover raster layer of each crop year to identify and filter out the small isolated groups of pixels, which were considered 'noise'. The groups of six pixels or less (<0.5 ha) were considered unlikely to belong to any managed irrigated crop or pasture.

Table 2. Land cover classification criteria.

Land Cover Description	Binary Class PID Based on Ts - Ta and NDVI		
	Spring	Summer	Autumn
Single-season active:			
Spring active	S4, S3 *	S1, S2	S1, S2
Summer active	S1, S2	S4, S3 *	S1, S2
Autumn active	S1, S2	S1, S2	S4, S3 *
Two-season active:			
Spring–Summer	S4, S3 *	S4, S3 *	S1, S2
Spring & Autumn	S4, S3 *	S1, S2	S4, S3 *
Summer–Autumn	S1, S2	S4, S3 *	S4, S3 *
All-season active:			
Perennially Active#	S4	S4	S4

PID = Pixel identification (See Figure 3); * Spatial context to consider S3 with S4. # Pixel with two S4 seasons and one S3 season considered as perennially active.

3.4. Step 4: Evaluating the Irrigated Land Cover Changes

To evaluate the temporal changes, maps and diagrams were generated using the pixel level land cover classes of each crop year. Maps of irrigated land cover classes were prepared for visual evaluation. Illustrations were created to show the changes of land cover classes for the total region as well as for the six individual irrigation sub-regions.

4. Results

Irrigation is the application of supplemental water to crops in order to maintain and enhance crop growth. Therefore, in the management of irrigation due consideration is given to the amount of irrigation water that is to be applied to meet the crop water demand. As the crop water demand varies due to multiple factors including crop type, phenology and evapotranspiration [34], the irrigation application also varies. In the North-Central Victoria, we have identified seven types of irrigated land cover (Table 2). The land which is actively irrigated throughout all seasons is designated as 'perennially active', which refers to either perennial pasture (e.g., perennial ryegrass) or perennial horticulture crop. Other land areas are seasonally irrigated in one or two seasons (Table 2), which refer to either annual pasture, annual horticulture or seasonal crop.

To check the accuracy of whether a land parcel was 'irrigated' or not, we used the 2018-19 summer season data sets. An accuracy assessment was carried out at the farm level (irrigation water delivery unit). Figure 5 shows the spread of farms selected for accuracy assessment. Farms receiving ≤10 mL of water within this season were considered as not actively managed for plant production and were excluded from accuracy assessment. All farms that received irrigation water deliveries during this period were treated as 'irrigated' and others as 'non-irrigated'. These were taken as a 'reference' indicating 'actual' irrigation occurrence. The farms with an area (≥1 ha) identified as actively irrigated ('S4') were considered as 'estimates'. Altogether, 5650 farms were selected for accuracy assessment. Producer's and user's accuracies were calculated as per standard procedure [35,36]. Table 3 shows the results of the accuracy assessment. The values in Table 3a are the number of farms. The values in Table 3b are the proportion (%) of farms. The overall accuracy was 95.7 percent.

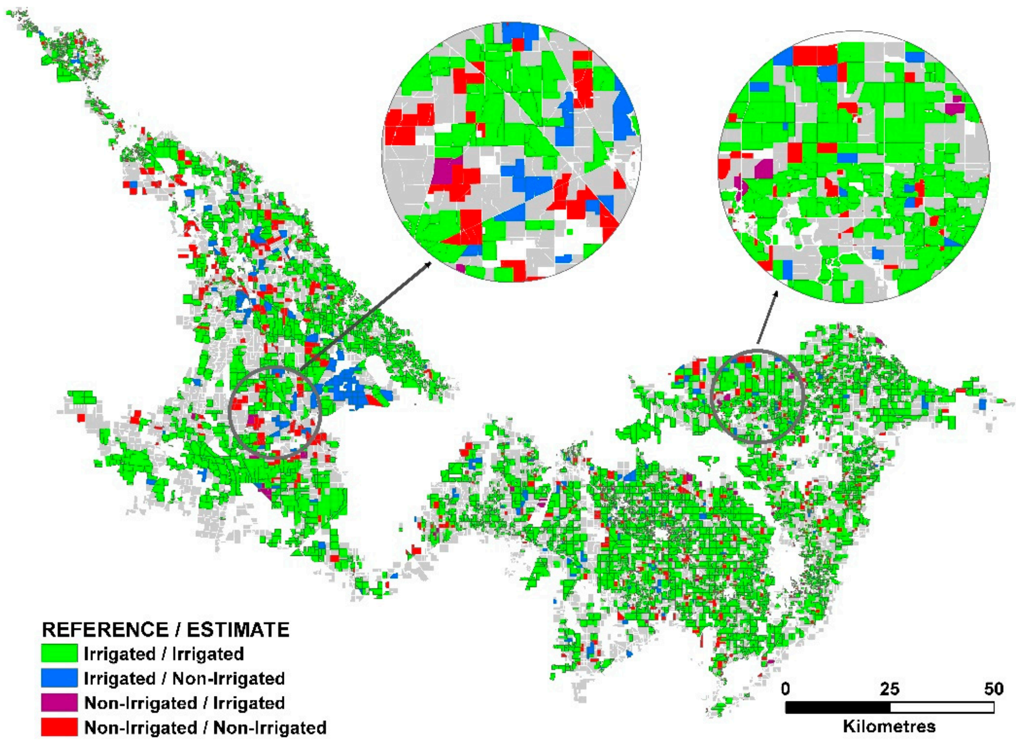

Figure 5. Map showing the accuracy assessment of farms.

Table 3. Accuracy Assessment of the Irrigation Classification.

a. Occurrence		
Classification (Image Analysis)	**Reference (Water Delivery Records)**	
	Irrigated	**Non-Irrigated**
Irrigated	4472	47
Non-Irrigated	196	935
b. Accuracy		
	Producer's Accuracy (%)	**User's Accuracy (%)**
Irrigated	95.8	99.0
Non-Irrigated	95.2	82.7

Overall Accuracy = 95.7%.

In the sub-sections below, we present the temporal changes in irrigated land cover at regional as well as sub-regional levels. Also, we present the changes in an important land cover class (i.e., 'perennially active') that has significant implications for dairy pastures and perennial horticulture.

4.1. Regional Changes

Figure 6 show the maps of irrigated land cover of a representative subregion (Central-Goulburn) in the study area during 2008–2009 to 2018–2019. These maps show considerable changes in land cover from year to year. The 2008–2009 crop year marks the end of an extreme dry period in the southeast Australia, known as the Millennium Drought [37]. The total area of irrigated land cover in 2008–2009 was very low due to the drought-induced water scarcity. As Figure 7A shows, in subsequent years, irrigated area increased from about 200,000 ha in 2008–2009 to about 557,000 ha in 2009–2010 and to about 660,000 ha in 2012–2013. Post-2012–2013, there has been a slow but consistent decline in the irrigated area. The irrigated land cover in 2018–2019 was almost half (354,000 ha) of what it was in 2012–2013 (Figure 7A).

The stack diagram (Figure 7B) shows the changes in the seven irrigated land cover classes over the years. The biggest increase from 2008–2009 to 2012–2013 was in the 'spring active' class. The 'perennially active' and 'spring & autumn active' classes had moderate increases but after 2012–2013, these two classes had very little change. The 'autumn active' and 'spring active' classes showed noticeable variations over the years.

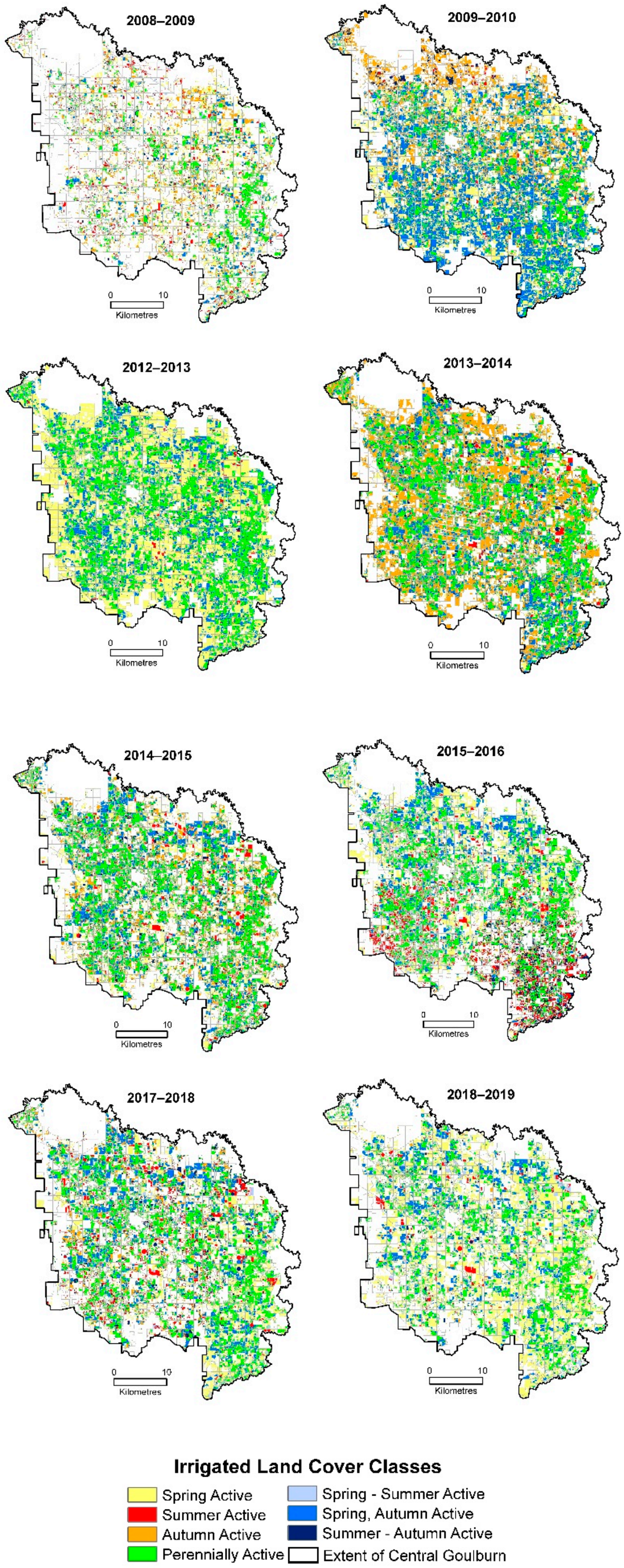

Figure 6. Maps of irrigated land cover in the Central-Goulburn region from 2008–2009 to 2018–2019.

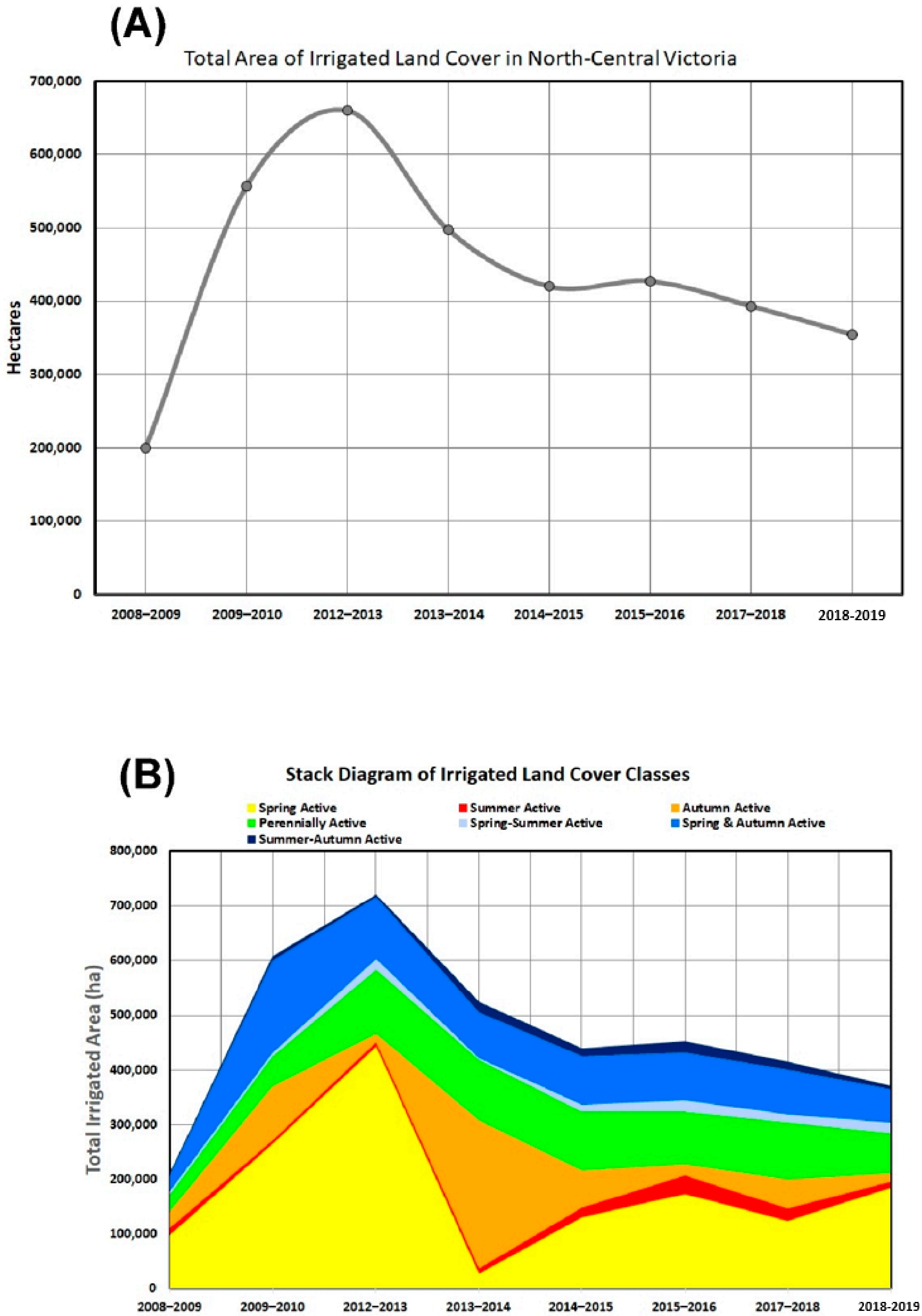

Figure 7. Changes in irrigated land cover in North-Central Victoria from 2008–2009 to 2018–2019. (**A**) Changes in total area over the years. (**B**) Stack diagram showing changes in seven land cover classes.

4.2. Changes in Sub-Regions

The six sub-regions experienced changes in the area of irrigated land cover with moderate differences (Figure 8). Pyramid–Boort and Torrumbarry, located in the western part, appeared to have recovered from drought sooner than the rest of the region. Irrigated land in Pyramid–Boort sub-region increased from a minimum (47,000 ha) in 2008–2009 to a maximum (160,000 ha) in 2009–2010. Similarly, the Torrumbarry sub-region had a substantial increase in irrigated land from about 30,000 ha in 2008–2009 to about 100,000 ha in 2009–2010 and to a maximum of 104,000 ha in 2012–2013. Though the other four sub-regions (Central Goulburn, Shepparton, Campaspe and Murray Valley) were similar in having the maximum irrigated land in 2012–2013, they differed in the proportion of decrease in subsequent years (Figure 8).

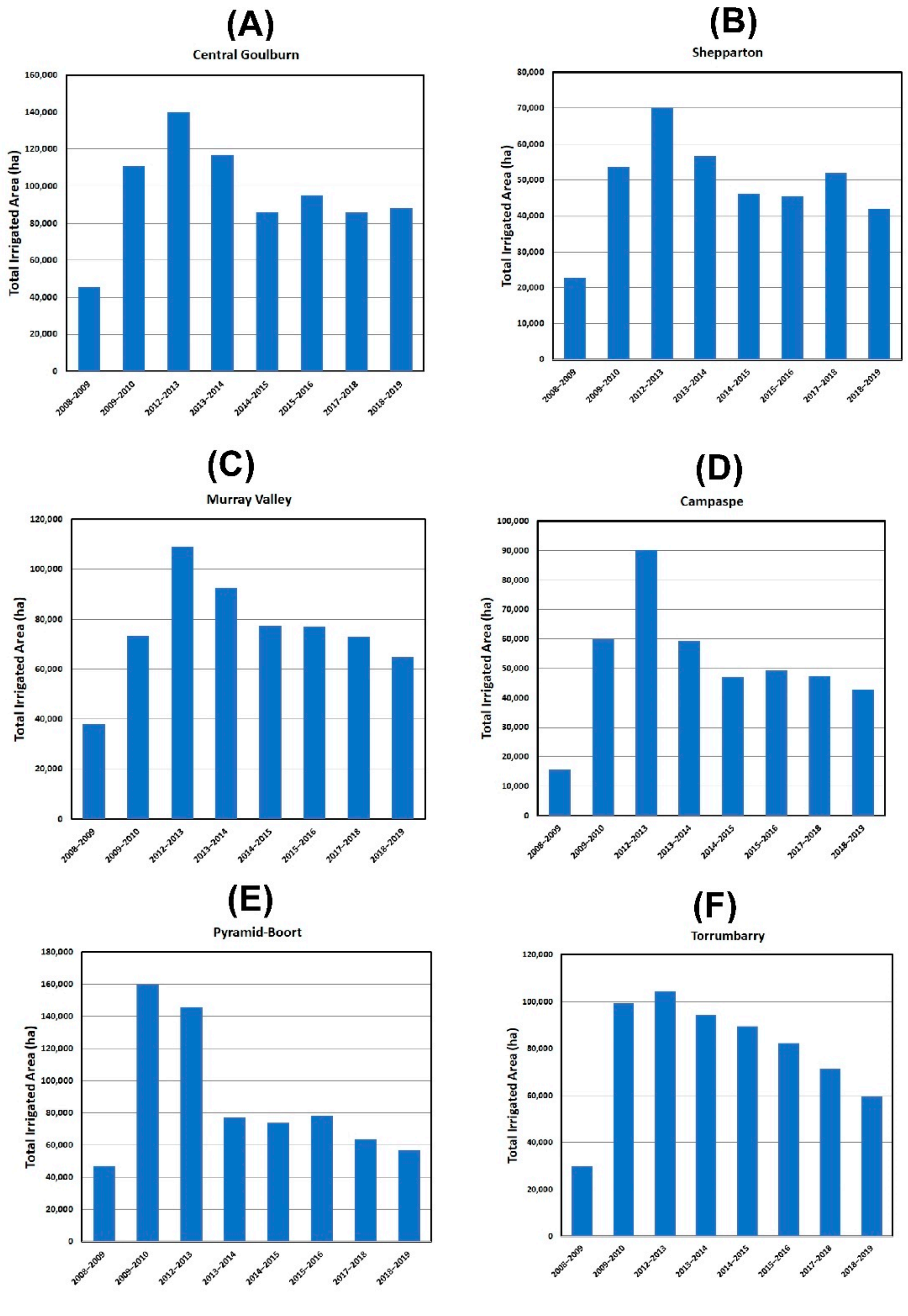

Figure 8. Changes in irrigated land cover of six irrigated sub-regions in North-Central Victoria during 2008–2009 and 2018–2019. (**A**) Central Goulburn; (**B**) Shepparton; (**C**) Murray Valley; (**D**) Campaspe; (**E**) Pyramid-Boort; and (**F**) Torrumbarry.

4.3. Changes in Perennially Active Class across Sub-Regions

A large proportion of 'perennially active' land cover class is occupied by perennial pasture (*Lolium perenne* L.) followed by perennial horticulture. Changes in irrigation over the last 10 years have been driven by several factors including seasonal extremes, commodity prices and policy reforms in agriculture. However, these changes in irrigated land cover are not uniform across the region.

Figure 9 shows the level of changes that occurred in the surface area occupied by the perennially active class of land cover in the six sub-regions during the study period.

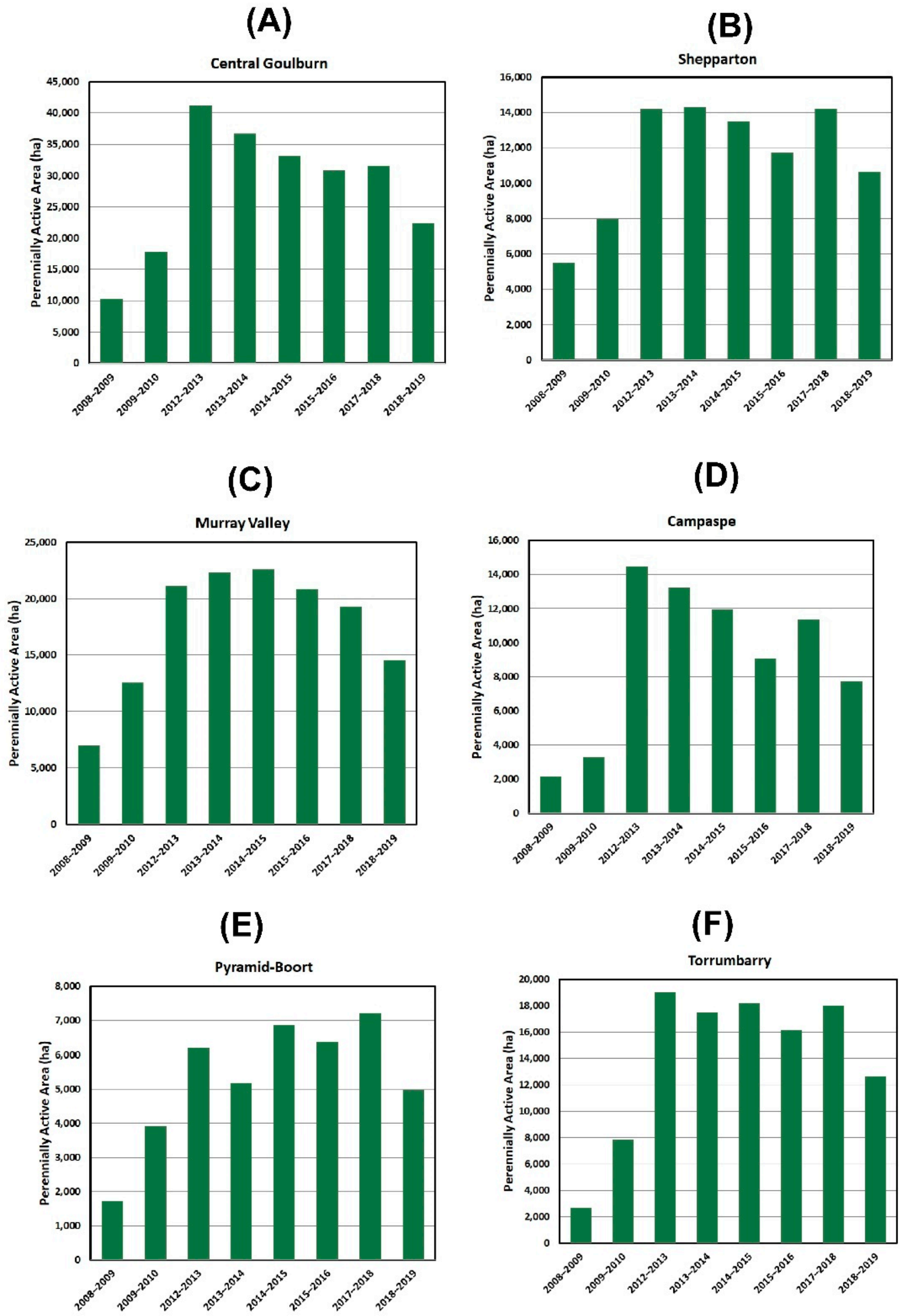

Figure 9. Temporal changes in the Perennially Active class of irrigated land cover. (**A**) Central Goulburn; (**B**) Shepparton; (**C**) Murray Valley; (**D**) Campaspe; (**E**) Pyramid-Boort; and (**F**) Torrumbarry.

In Central Goulburn, the total area of perennially active class in 2008–2009 was approximately 10,000 ha, which increased to over 40,000 ha in 2013–2014. Thereafter, there has been a consistent decline, reaching down to approximately 22,000 ha in 2018–2019 (Figure 9A). The decline may be attributed to the trend of transition from dairy to annual horticulture in this sub-region. Still a large proportion of irrigation water here is used by dairy farmers [38].

In Shepparton Sub-region, total area of perennially active class in 2008–2009 was a little over 5000 ha, which increased to approximately 8000 ha in 2009–2010 and to 14,000 ha in 2012–2013. The changes in the subsequent years have not been uniform though area was reduced to approximately 10,000 ha in 2018–2019 (Figure 9B). There has been a reduction in dairy in the last five years, transitioning to non-dairy activities including mixed farming and cropping [38].

In Murray Valley, the area of perennially active class in 2008–2009 was approximately 7,000 ha, which increased in the subsequent years, reaching up to approximately 22,500 ha in 2014–2015. Thereafter there was a decline in area, reaching down to approximately 14,500 ha in 2018–2019 (Figure 9C). There has been a reduction in dairy and perennial horticulture industries during the last five years. A transition from dairy to cropping has occurred in this sub-region as well [38].

In the Campaspe Sub-region, the area of perennially active class was very low in 2008–2009 and 2009–2010 (between 2000 and 3000 ha). It increased to approximately 14,500 ha in 2012–2013. In subsequent years, though the changes have been uneven, the area declined to approximately 7700 ha in 2018–2019 (Figure 9D). The decline is related to the reduction in dairy industry in recent years. This sub-region is more known for cropping and mixed farming than for dairying [38].

The Pyramid–Boort Sub-region has the highest extent of cropping land use in the region. Other dominant land use is mixed farming. Dairying is limited with notable reduction especially found in the south-east in the recent past [38]. This is reflected in the relatively low area of perennially active class, which was approximately 7000 ha in 2017–2018 and 5000 ha in 2018–2019 (Figure 9E).

In the past few years, there has been some decrease in dairy industry in the central and south-eastern half of Torrumbarry. This did not create dramatic changes in the total area of perennially active class from 2012–2013 until 2017–2018, ranging between 17,000 ha and 19,000 ha. However, in 2018–2019, the area was reduced to approximately 12,500 ha (Figure 7F). Recently, mixed farming and grazing have increased in this sub-region [38].

5. Discussion

The study area is part of the Murray-Darling Basin (MDB). In MDB, there are highly regulated water management provisions, which are used to provide a reliable and equitable supply of water for irrigation and other uses. Recent regulations have strengthened the legal, market and price aspects of water supply. This has incentivized irrigators to achieve irrigation efficiencies. Irrigators have water entitlements of nominal volume of water to use. However, to accommodate the year-to-year variability in the amount of water available, annual allocations are changed. As a result, in years of drought, the nominal volume of water entitlement may be very low. During the millennium drought annual allocations fell to as low as 10% of the pre-drought entitlements [39]. The effect of low water availability was reflected in the low area of the 2008–2009 irrigated land cover estimated in this study.

This study presented the application of relative differences in temperature and vegetation to identify and monitor actual irrigated areas. Relating low surface temperature and high vegetation cover to irrigated crops is not a new concept [31,40–42]. However, it was only after the space-borne thermal sensors became available that regional scale studies became possible. Temperatures derived from the Landsat series (L5, L7 and L8) and ASTER are suitable for farm level agricultural studies, both in terms of large regional coverage and appropriate spatial resolution, as presented in this study. The coarse resolution thermal bands (e.g., MODIS and AVHRR), though not ideal for farm scale studies, are useful to provide information at regional and landscape levels. More recently, surface temperatures from the Ecosystem Spaceborne Thermal Radiometer Experiment on Space Station (ECOSTRESS) at 60 m spatial resolution have offered increased opportunities for studies in irrigated agriculture [43].

Vegetation cover (NDVI) at medium to fine resolution is readily available from several satellites (e.g., Sentinel-2, SPOT, RapidEye, QuickBird and WorldView). However, synchronous delivery of vegetation cover and surface temperature is available only from Landsat and ASTER. In some circumstances, vegetation cover (NDVI) alone may provide some indication of irrigated land but to investigate in-season changes in irrigation, temperature differences are needed. If the study area is large with heterogenous climatic conditions, surface temperature may not provide the desired distinction between irrigated and non-irrigated lands across the whole region. In such a situation, using the surface-air temperature difference is a better option.

The operational approach to map irrigated land cover used in this study is most suited to arid or semi-arid areas where rainfall is not a confounding factor. In this study area, the rainfall totals varied from year to year and from season to season (Figure 10). Occasional spikes in rainfall were unlikely to influence the results of this study because the seasonal totals were not high enough to meet the crop water demand.

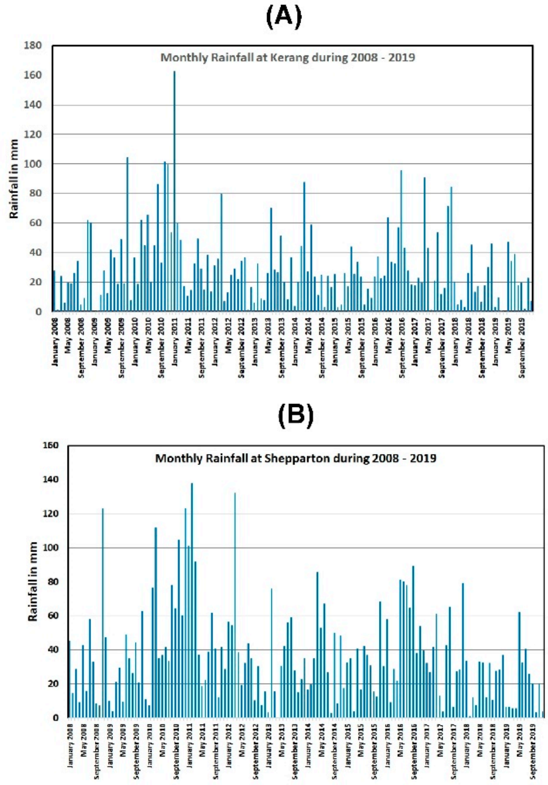

Figure 10. Monthly totals of rainfall during 2008–2009 and 2018–2019. (**A**) Kerang weather station (35.72° S; 143.92° E) located in the north-west of the study area. (**B**) Shepparton weather station (36.43° S; 145.39° E) located in the south-east of the study area.

The initial threshold of 0.4 was adopted for the bilevel segmentation of NDVI in this study on the assumption that any vegetation under 0.4 NDVI is not a managed crop or pasture. However, the initial threshold for Ts - Ta was the median value of Ts - Ta, which varied as per the surface and air temperatures at the time of image acquisition. The aim was to identify pixels on the basis of 'relative differences' in Ts - Ta. The assumption was that the relatively cool pixels indicated 'irrigation' and the relatively warm pixels indicated the absence of irrigation. This assumption holds good if a large proportion of area under study is agricultural land with no major features of climatic extremes as is the case in this study. The relative differences in Ts - Ta were meant to seek distinction between two situations i.e., (1) Actively irrigated land, and (2) Land with no active irrigation and/or rainfed area.

It is desired that the Ts - Ta threshold and its range is revisited if significant changes occur in the land cover composition in the study area.

The study area is dominated by irrigated pastures (87% of irrigated land). The key assumption made about irrigated pasture, unlike dryland pasture, is that the greenness is maintained throughout the season to almost a uniform level, by applying irrigation as required. It is therefore sufficient to use one satellite image to represent an irrigation period, as done in this study. Similarly, for irrigated horticulture crops, the key assumption is that irrigation is used to maintain an optimal level of root zone moisture throughout period of canopy growth. Therefore, the use of one image per season is considered adequate to capture irrigation activity. Our decision to use a single image per irrigation period was in accordance with previous studies. In a study conducted previously on the perennial horticulture crops in the same region, it was found that the use of single 'midseason' image is adequate to assess maximum crop cover because of strong temporal stability in NDVI response (O'Connell 2011, p. 61) [44]. Quoting multiple studies, Velpuri et al. (2009, p. 1384) [45] reported that "single date fine-resolution imagery, acquired at critical growth stages, is sufficient to identify irrigation". However, minor temporal fluctuations in vegetation cover within a season are possible due to certain factors including over-grazing of pastures, onset of crop disease or extreme weather events. Severe cases of temporal fluctuations may warrant more than one image per season for land cover analysis.

6. Conclusions

The synchronous measures of surface temperature and vegetation cover based on the satellite images from the Landsat series (L-5, L-7 and L-8) and ASTER were found to be suitable to distinguish between irrigated and non-irrigated pasture/crop to an overall accuracy of 95.7% in the North-Central Victoria, Australia. The irrigation profiles of spring, summer and autumn seasons defined by the combined binary classes of the two measures (Ts - Ta and NDVI) were useful for land cover classification, indicating actual irrigation practices prevalent during 2008–2009 and 2018–2019. Active irrigation varied considerably over the years. Following an extreme dry period in the region, the 2008–2009 crop year had the lowest total irrigated area (about 200,000 ha) which increased more than three-fold in 2012–2013 (about 660,000 ha). Thereafter, the region witnessed a steady decline in irrigation, reducing to about 354,000 ha in 2018–2019.

Author Contributions: Conceptualization, M.A., A.M. and D.W.; methodology, M.A. and D.W.; formal analysis, M.A., A.M., K.S. and D.W.; writing—original draft preparation, M.A.; writing—review and editing, M.A., A.M., D.W. and K.S. All authors have read and agreed to the published version of the manuscript.

Funding: This research received no external funding.

Acknowledgments: Thanks are due to the colleagues in Agriculture Victoria Research (AVR), Department of Jobs, Precincts and Regions (DJPR), for their support for this work.

Conflicts of Interest: The authors declare no conflict of interest.

References

1. Colaizzi, P.; Bliesner, R.; Hardy, L. A Review of Evolving Critical Priorities for Irrigated Agriculture. In *World Environmental and Water Resources Congress 2008*; Raymond 1-15; Roger, W., Babcock, W., Jr., Eds.; American Society of Civil Engineers: Reston, VA, USA, 2008.
2. World Bank. "Water in Agriculture." World Bank. Available online: https://www.worldbank.org/en/topic/water-in-agriculture (accessed on 6 July 2020).
3. Weiss, M.; Jacob, F.; Duveiller, G. Remote Sensing for Agricultural Applications: A Meta-Review. *Remote Sens. Environ.* **2020**, *236*, 111402. [CrossRef]
4. Aleksandrova, M.; Lamers, J.P.; Martius, C.; Tischbein, B. Rural Vulnerability to Environmental Change in the Irrigated Lowlands of Central Asia and Options for Policy-Makers: A Review. *Environ. Sci. Policy* **2014**, *41*, 77–88. [CrossRef]
5. Alvino, A.; Marino, S. Remote Sensing for Irrigation of Horticultural Crops. *Horticulturae* **2017**, *3*, 40. [CrossRef]

6. Santos, C.; Lorite, I.J.; Tasumi, M.; Allen, R.G.; Fereres, E. Integrating Satellite-Based Evapotranspiration with Simulation Models for Irrigation Management at the Scheme Level. *Irrig. Sci.* **2008**, *26*, 277–288. [CrossRef]
7. Ozdogan, M.; Yang, Y.; Allez, G.; Cervantes, C. Remote Sensing of Irrigated Agriculture: Opportunities and Challenges. *Remote Sens.* **2010**, *2*, 2274–2304. [CrossRef]
8. Hatfield, J.L.; Prueger, J.H.; Sauer, T.J.; Dold, C.; O'Brien, P.; Wacha, K. Applications of Vegetative Indices from Remote Sensing to Agriculture: Past and Future. *Inventions* **2019**, *4*, 71. [CrossRef]
9. Thenkabail, P.S.; Schull, M.; Turral, H. Ganges and Indus River Basin Land Use/Land Cover (LULC) and Irrigated Area Mapping Using Continuous Streams of MODIS Data. *Remote Sens. Environ.* **2005**, *95*, 317–341. [CrossRef]
10. Xiao, X.; Boles, S.; Liu, J.; Zhuang, D.; Frolking, S.; Li, C.; Salas, W.; Moore, B., III. Mapping Paddy Rice Agriculture in Southern China Using Multi-Temporal MODIS Images. *Remote Sens. Environ.* **2005**, *95*, 480–492. [CrossRef]
11. Biggs, T.W.; Thenkabail, P.S.; Gumma, M.K.; Scott, C.A.; Parthasaradhi, G.R.; Turral, H.N. Irrigated Area Mapping in Heterogeneous Landscapes with MODIS Time Series, Ground Truth and Census Data, Krishna Basin, India. *Int. J. Remote Sens.* **2006**, *27*, 4245–4266. [CrossRef]
12. Alexandridis, T.K.; Zalidis, G.C.; Silleos, N.G. Mapping Irrigated Area in Mediterranean Basins Using Low Cost Satellite Earth Observation. *Comput. Electron. Agric.* **2008**, *64*, 93–103. [CrossRef]
13. Ozdogan, M.; Gutman, G. A New Methodology to Map Irrigated Areas Using Multi-Temporal MODIS and Ancillary Data: An Application Example in the Continental Us. *Remote Sens. Environ.* **2008**, *112*, 3520–3537. [CrossRef]
14. Dheeravath, V.; Thenkabail, P.S.; Chandrakantha, G.; Noojipady, P.; Reddy, G.P.O.; Biradar, C.M.; Gumma, M.K.; Velpuri, M. Irrigated Areas of India Derived Using Modis 500 M Time Series for the Years 2001–2003. *Isprs J. Photogramm. Remote Sens.* **2010**, *65*, 42–59. [CrossRef]
15. Loveland, T.R.; Reed, B.C.; Brown, J.F.; Ohlen, D.O.; Zhu, Z.; Yang, L.; Merchant, J.W. Development of a Global Land Cover Characteristics Database and IGBP Discover from 1 Km AVHRR Data. *Int. J. Remote Sens.* **2000**, *21*, 1303–1330. [CrossRef]
16. Arino, O.; Gross, D.; Ranera, F.; Leroy, M.; Bicheron, P.; Brockman, C.; Defourny, P.; Vancutsem, C.; Achard, F.; Durieux, L.; et al. Globcover: Esa Service for Global Land Cover from MERIS. In Proceedings of the 2007 IEEE International Geoscience and Remote Sensing Symposium, Barcelona, Spain, 23–28 July 2007.
17. hen, Y.; Feng, X.; Fu, B.; Shi, W.; Yin, L.; Lv, Y. Recent Global Cropland Water Consumption Constrained by Observations. *Water Resour. Res.* **2019**, *55*, 3708–3738.
18. Thenkabail, P.S.; Knox, J.W.; Ozdogan, M.; Gumma, M.K.; Congalton, R.G.; Wu, Z.T.; Milesi, C.; Finkral, A.; Marshall, M.; Mariotto, I.; et al. Assessing Future Risks to Agricultural Productivity, Water Resources and Food Security: How Can Remote Sensing Help? *Photogramm. Eng. Remote Sens.* **2012**, *78*, 774–782.
19. Thenkabail, P.S.; Wu, Z. An Automated Cropland Classification Algorithm (ACCA) for Tajikistan by Combining Landsat, Modis, and Secondary Data. *Remote Sens.* **2012**, *4*, 2890–2918. [CrossRef]
20. Jordan, C.F. Derivation of Leaf-Area Index from Quality of Light on the Forest Floor. *Ecology* **1969**, *50*, 663–666. [CrossRef]
21. Rouse, J.W.; Haas, R.H.; Schell, J.A.; Deering, D.W. Monitoring Vegetation Systems in the Great Plains with Erts. In *Third ERTS Symposium, 309–317*; NASA: Washington, DC, USA, 1973.
22. González-Dugo, M.P.; Moran, M.S.; Mateos, L.; Bryant, R. Canopy Temperature Variability as an Indicator of Crop Water Stress Severity. *Irrig. Sci.* **2006**, *24*, 233–240. [CrossRef]
23. G-MW. Goulburn-Murray Irrigation District. Goulburn-Murray Water. Available online: https://www.g-mwater.com.au/downloads/gmw/MTR/TATDOC-_4079268-v1-fact_sheet_-_GMID_-_november_2015.PDF (accessed on 8 July 2020).
24. Abuzar, M.; McAllister, A.; Whitfield, D. Mapping Irrigated Farmlands Using Vegetation and Thermal Thresholds Derived from Landsat and Aster Data in an Irrigation District of Australia. *Photogramm. Eng. Remote Sens.* **2015**, *81*, 229–238.
25. Miura, T.; Turner, J.P.; Huete, A.R. Spectral Compatibility of the NDVI across VIIRS, MODIS, and AVHRR: An Analysis of Atmospheric Effects Using EO-1 Hyperion. *Geosci. Remote Sens. IEEE Trans.* **2013**, *51*, 1349–1359. [CrossRef]
26. Chander, G.; Markham, B.L.; Helder, D.L. Summary of Current Radiometric Calibration Coefficients for Landsat MSS, TM, ETM+, and EO-1 ALI Sensors. *Remote Sens. Environ.* **2009**, *113*, 893–903. [CrossRef]

27. USGS. Using the USGS Landsat Level-1 Data Product. USGS. Available online: https://www.usgs.gov/land-resources/nli/landsat/using-usgs-landsat-level-1-data-product (accessed on 8 July 2020).
28. Abrams, M.; Hook, S.; Ramachandran, B. *Aster User Handbook, Version 2. JPL*; NASA: Washington, DC, USA, 2002.
29. ESA. *Sentinel-2 User Handbook*; European Space Agency: Paris, France, 2015.
30. Abuzar, M.; Whitfield, D.; McAllister, A.; Sheffield, K. Application of ET-NDVI-Relationship Approach and Soil-Water-Balance Modelling for the Monitoring of Irrigation Performance of Treed Horticulture Crops in a Key Fruit-Growing District of Australia. *Int. J. Remote Sens.* **2019**, *40*, 4724–4742. [CrossRef]
31. Idso, S.B.; Jackson, R.D.; Pinter, P.J., Jr.; Reginato, R.J.; Hatfield, J.L. Normalizing the Stress-Degree-Day Parameter for Environmental Variability. *Agric. Meteorol.* **1981**, *24*, 45–55. [CrossRef]
32. Jackson, R. Canopy Temperature and Crop Water Stress. *Adv. Irrig.* **1982**, *1*, 43–85.
33. Otsu, N. A Threshold Selection Method from Gray-Level Histograms. *Syst. Man Cybern. IEEE Trans.* **1979**, *9*, 62–66. [CrossRef]
34. Allen, R.G.; Pereira, L.S.; Raes, D.; Smith, M. *Crop Evapotranspiration: Guidelines for Computing Crop Water Requirements, Fao Irrigation and Drainage Paper 56*; FAO: Rome, Italy, 1998.
35. Congalton, R.G. A Review of Assessing the Accuracy of Classifications of Remotely Sensed Data. *Remote Sens. Environ.* **1991**, *37*, 35–46. [CrossRef]
36. Foody, G.M. Status of Land Cover Classification Accuracy Assessment. *Remote Sens. Environ.* **2002**, *80*, 185–201. [CrossRef]
37. Van Dijk, A.I.; Beck, H.E.; Crosbie, R.S.; de Jeu, R.A.; Liu, Y.Y.; Podger, G.M.; Timbal, B.; Viney, N.R. The Millennium Drought in Southeast Australia (2001–2009): Natural and Human Causes and Implications for Water Resources, Ecosystems, Economy, and Society. *Water Resour. Res.* **2013**, *49*, 1040–1057. [CrossRef]
38. State of Victoria. *Regional Irrigated Land and Water Use Mapping in the Goulburn Murray Irrigation District-Technical Report*; Shepparton: Victoria, Australia, 2020.
39. Kirby, M. Irrigation. In *Water*; Prosser, I.P., Ed.; CSIRO Publishing: Victoria, Australia, 2011; pp. 105–118.
40. Moran, M.S.; Clarke, T.R.; Inoue, Y.; Vidal, A. Estimating Crop Water Deficit Using the Relation between Surface-Air Temperature and Spectral Vegetation Index. *Remote Sens. Environ.* **1994**, *49*, 246–263. [CrossRef]
41. Maas, S.J.; Vanderbilt, V.C.; Barnes, E.M.; Miller, S.N.; Clarke, T.R. Application of Image-Based Remote Sensing to Irrigated Agriculture. In *Remote Sensing for Natural Resources Management and Environmental Monitoring: Manual of Remote Sensing*; Susan, U., Ed.; John Wiley & Sons: Hoboken, NJ, USA, 2004; pp. 617–676.
42. Petropolous, G.; Carlson, T.N.; Wooster, M.J.; Islam, S. A Review of Ts/VI Remote Sensing Based Methods for the Retrieval of Land Surface Energy Fluxes and Soil Surface Moisture. *Prog. Phys. Geogr.* **2009**, *33*, 224–250. [CrossRef]
43. Fisher, J.B.; Lee, B.; Purdy, A.J.; Halverson, G.H.; Dohlen, M.B.; Cawse-Nicholson, K.; Wang, A.; Anderson, R.G.; Aragon, B.; Arain, M.A.; et al. ECOSTRESS: NASA's Next Generation Mission to Measure Evapotranspiration from the International Space Station. *Water Resour. Res.* **2020**, *56*, e2019WR026058. [CrossRef]
44. O'Connell, M.G. Satellite Based Yield: Water Use Relationships of Perennial Horticultural Crops. Ph.D. Thesis, University of Melbourne, Melbourne, Australia, 2011.
45. Velpuri, N.M.; Thenkabail, P.S.; Gumma, M.K.; Biradar, C.M.; Dheeravath, V.; Noojipady, P.; Yuanjie, L. Influence of Resolution in Irrigated Area Mapping and Area Estimations. *Photogramm. Eng. Remote Sens.* **2009**, *75*, 1383–1395. [CrossRef]